Turkish Journal of Electrical Engineering & Computer Sciences

http://journals.tubitak.gov.tr/elektrik/

Research Article

Turk J Elec Eng & Comp Sci
(2016) 24: 590 – 604

doi:10.3906/elk-1309-231

Research on switched reluctance machine drive topology and control strategies for electric vehicles

He CHENG, Hao CHEN*, Lei MA, Guojun YU
School of Information and Electrical Engineering, China University of Mining and Technology, Xuzhou, Jiangsu, P.R. China

Received: 30.09.2013 • **Accepted/Published Online:** 19.12.2013 • **Final Version:** 05.02.2016

Abstract: The electric drive system is one of the key technologies for electric vehicles. First, the energy flow of an electric vehicle is analyzed in the driving, braking, and charging working states. After that, a drive topology that can achieve 3 working states is proposed based on the driving characteristics of a switched reluctance machine. In the driving state, the boost mode of a front-end converter is used to achieve different operating conditions, including low speed with a light load or high speed with a heavy load. In the braking state, the front-end converter is used to implement smooth switching between initial excitation and braking energy feedback. In the charging state, a new power factor correction circuit is proposed, and the motor windings and power converter constitute the onboard charger, whose power factor is correctable. According to the proposed drive topology, the control strategies for 3 working states are put forward. Finally, an experimental platform is built to verify the correctness of the control strategies as well as the flexibility of the whole system.

Key words: Electric vehicle, switched reluctance machine, drive topology, onboard charger, power factor correction

1. Introduction

With the advantages of high fuel efficiency, less pollution emission, and the ability to absorb braking energy, hybrid electric vehicles (HEVs) and electric vehicles (EVs) are increasingly becoming popular in transportation due to the pressures of fuel consumption and environmental pollution [1,2]. The electric drive system, whose function is to convert electrical energy into mechanical energy, is one of the most important parts of the EV, and it needs to possess the characteristics of high efficiency and high reliability. The switched reluctance machine (SRM) has a simple structure, robustness, a high starting torque, a wide speed range, high efficiency, great fault tolerance, and 4-quadrant operation [3,4], all of which indicate its suitability for EV applications [5–9].

For a battery-powered EV, a front-end DC/DC converter can boost the supply voltage, decrease the supply current, reduce the volume of the power converter, and improve efficiency. It can also reduce the impact of battery voltage fluctuation and back electromotive force (EMF) on driving performance. In [10], a bidirectional DC/DC converter was used to maintain the common DC-link voltage constant for a battery energy storage system. However, no control strategy was proposed. In [11], a bidirectional buck-boost converter was used to transfer energy between the ultracapacitor and the battery, which can improve the acceleration performance of the EV as well as the service life and efficiency of the storage battery.

An onboard charger, composed of motor windings and a power converter, can reduce the cost and increase

*Correspondence: chenhaocumt@tom.com

the flexibility of charging [12–14]. In [12], the asynchronous machine windings with an external rectifier and a LC filter constituted the DC/DC boost circuit for battery charging. The battery charger is was created with the same power devices used in an EV propulsion drive. However, external circuits are still needed. In [13], SRM windings are were employed as part of the charger, but the motor windings need a specific design. The charger also needs an external circuit and its control is complicated. Moreover, the power factor correction (PFC) is not under consideration. In [14], an onboard integral battery charger with the function of PFC was developed. The charger is made up of 4-wheeled asynchronous motors and their inverters. Thus, it cannot be applied to a single-motor drive system.

In this paper, the energy flow of driving, braking, and charging is analyzed for EVs. A drive topology is proposed that can achieve 3 working states. A bidirectional buck-boost converter is added before a classical bridge power converter with the phase winding between two switches. The boost mode of the front-end converter is used for driving; the buck mode is used for regenerative braking; motor windings and a power converter are employed to constitute the onboard charger with the function of a PFC. Control strategies are proposed according to 3 working states. The control strategies and the whole system are experimentally verified.

2. Work states of an EV

An EV has 3 working states: driving, braking, and charging. The energy flows of the 3 working states are shown in Figure 1.

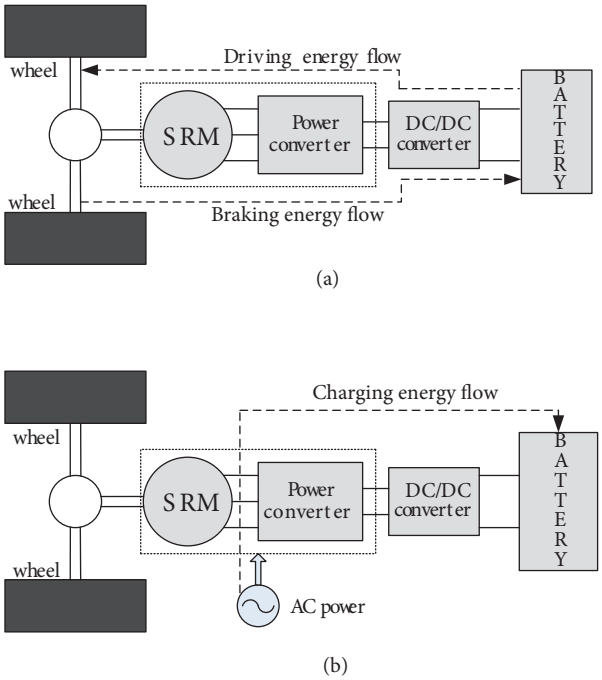

Figure 1. EV working states: (a) driving state and braking state, (b) charging state.

2.1. Driving state

As shown in Figure 1a, when the EV operates in the driving state, the battery is boosted by a front-end DC/DC converter, and then drives the EV by controlling a SRM as a motor. The electrical energy of the battery is converted into kinetic energy. The energy flows from the battery to the wheel.

2.2. Braking state

As shown in Figure 1a, when the EV operates in the braking state, the SRM operates as a generator. The battery is charged by the buck mode of the front-end DC/DC converter. The kinetic energy of the EV is converted into electrical energy. The energy flows from the wheel to the battery.

2.3. Charging state

As shown in Figure 1b, when the EV operates in the charging state, there is no conversion between electrical energy and kinetic energy. Motor windings and a power converter are employed to constitute the onboard charger to charge the battery, and no external components are needed. The energy flows from the AC power source to the battery.

3. EV drive topology

As shown in Figure 2, the drive topology is proposed to implement the aforementioned 3 working states. The battery is connected to a bidirectional DC/DC converter. The boost mode of the front-end converter is used to reduce the impact of battery voltage fluctuation on driving performance and enhance the SRM power output capability at high speeds in the driving state. In the braking state, the buck mode of the front-end converter is used to charge the battery. An asymmetrical half-bridge power converter is employed to achieve the 4-quadrant operation of the SRM. Motor windings L_a and L_b and power switches compose the onboard charger. The thick dashed lines in Figure 2 are the insertion of power cords in the charging state.

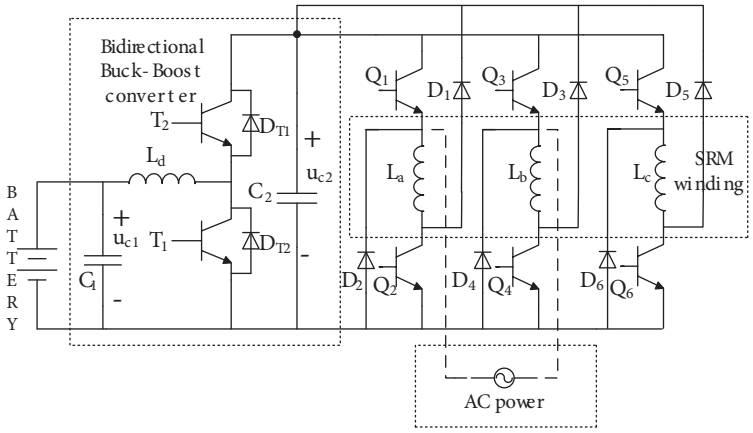

Figure 2. EV drive topology.

3.1. Driving state circuit

When an EV is in the driving state, switch T_2 is turned off. The equivalent circuit is shown in Figure 3. The front-end DC/DC converter works in boost mode; switch T_1 is activated to boost the battery voltage. The SRM is then driven by an asymmetrical half-bridge power converter.

3.2. Braking state circuit

When an EV is in the braking state, switch T_1 is turned off. The equivalent circuit is shown in Figure 4. The front-end DC/DC converter works in buck mode; switch T_2 is activated to charge the battery.

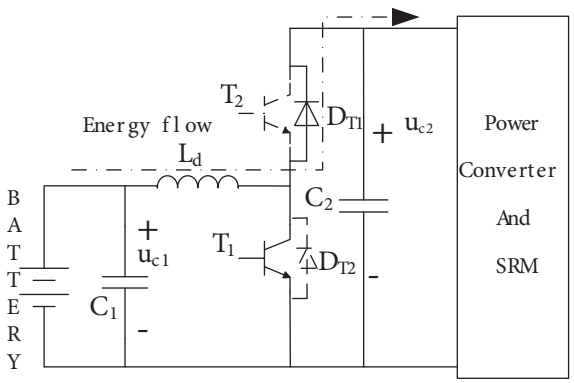

Figure 3. EV driving state equivalent circuit.

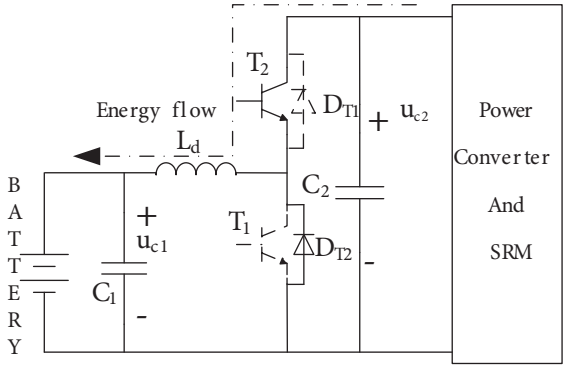

Figure 4. EV braking state equivalent circuit.

3.3. Charging state circuit

When an EV is in the charging state, switches T_1, Q_1, Q_3, Q_5, and Q_6 are turned off. The equivalent circuit is shown in Figure 5. Freewheeling diodes D_1, D_2, D_3, and D_4; switches Q_2 and Q_4; and SRM windings L_a and L_b make up the PFC circuit. Capacitor C_1, switch T_2, freewheeling diode D_{T2}, and winding L_d constitute the buck converter. The PFC circuit converts AC into DC with a high power factor. The battery is then charged by the buck converter.

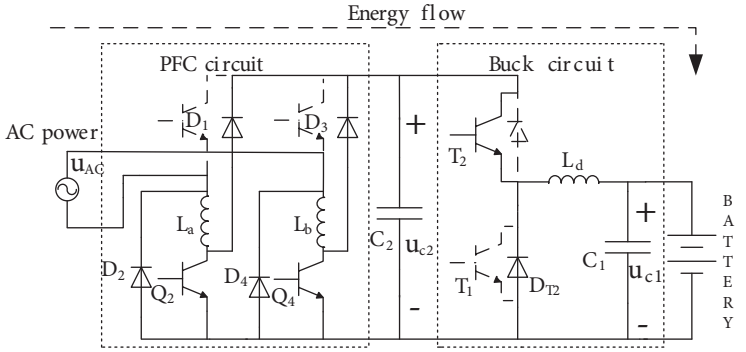

Figure 5. EV charging state equivalent circuit.

As shown in Figure 6, the PFC circuit operates in four operating modes. The $^-$ and α modes work in the positive half cycle of AC power as shown in Figure 6a, while β and χ modes work in the negative half cycle of AC power as shown in Figure 6b.

1) Mode $^-$: In the positive half cycle of AC power, switch Q_4 is turned on. The inductor current flows from the positive pole of the power source, going through winding L_b, switch Q_4, and freewheeling diode D_2, and then reaches the negative pole of the power source. During this process, the inductor current increases and the magnetic energy is stored in winding L_b.

2) Mode α: In the positive half cycle of AC power, switch Q_4 is turned off. The inductor current flows from the positive pole of the power source, going through winding L_b, freewheeling diode D_3, capacitor C_2, and freewheeling diode D_2, and then reaches the negative pole of the power source. During this process, the power and winding L_b deliver energy to capacitor C_2.

3) Mode β: In the negative half cycle of AC power, switch Q_2 is turned on. The inductor current flows from the positive pole of the power source, going through winding L_a, switch Q_2, and freewheeling diode D_4,

and then arrives at the negative pole of the power source. During this process, the inductor current increases and the magnetic energy is stored in winding L_a.

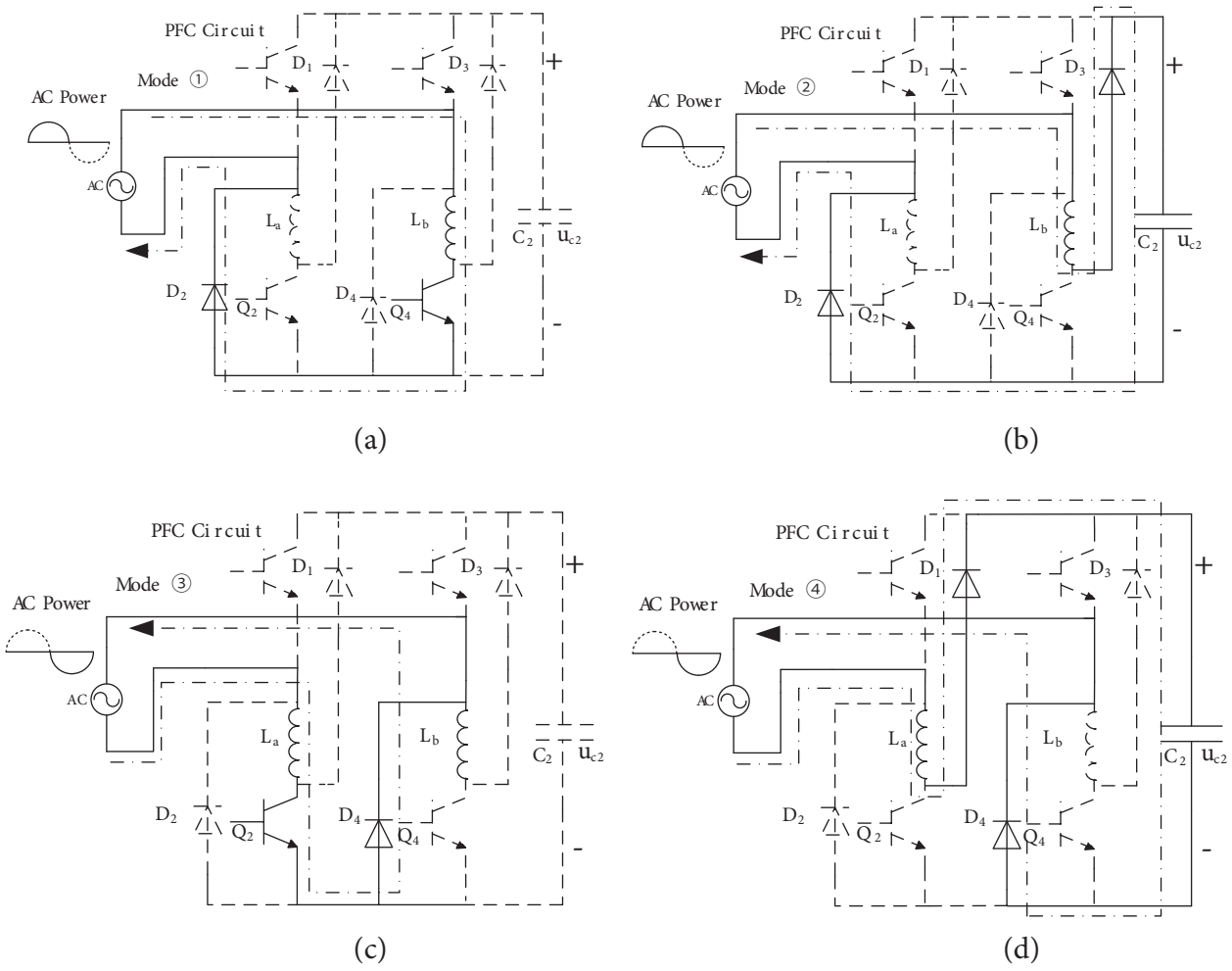

Figure 6. PFC circuit structure diagram: (a) mode ①, (b) mode α, (c) mode ②, (d) mode ③.

4) Mode χ: In the negative half cycle of AC power, switch Q_2 is turned off. The inductor current flows from the positive pole of the power source, going through winding L_a, freewheeling diode D_1, capacitor C_2, and freewheeling diode D_4, and then reaches the negative pole of the power source. During this process, the power and winding L_a deliver energy to capacitor C_2.

4. EV control strategies

EV has 3 working states, and every state has different control strategies based on different optimization goals.

Figure 7 shows the inductance curve of a SRM, a motoring current waveform, and a braking current waveform. θ_m is the position where the rotor teeth edge just starts to leave the stator teeth edge; θ_n is the position where the leading edge of the rotor pole is just aligned with the first edge of a stator pole; θ_u is the position where the rotor slot axis is aligned with the stator teeth axis; θ_a is the position where the rotor teeth axis is aligned with the stator teeth axis; and θ_m is set at 15° and θ_n is set at 30°.

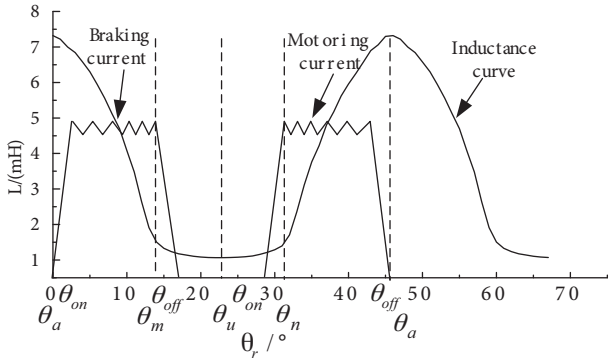

Figure 7. SRM inductance curve.

4.1. Control strategy for the driving state

Figure 8 shows the control structure diagram for an EV in driving mode. The SRM serves as a motor with an inner current loop and outer speed loop. Current chopper control (CCC) is applied at low speed. The speed regulator outputs reference I^* according to speed error ε_n. A hysteresis current regulator serves as an inner current regulator. As the speed increases, the back EMF of the SRM increases. The DC-link voltage is not sufficient to force the actual current to follow the reference current, and then angle position control (APC) is utilized at high speed. The conduction angle regulator has 2 functions. The optimized turn-on angle and turn-off angle are given when CCC is adopted at low speed; at high speed, the turn-off angle is fixed, the turn-on angle is adjusted to change the speed, and the logic synthesis circuit synthesizes all the signals.

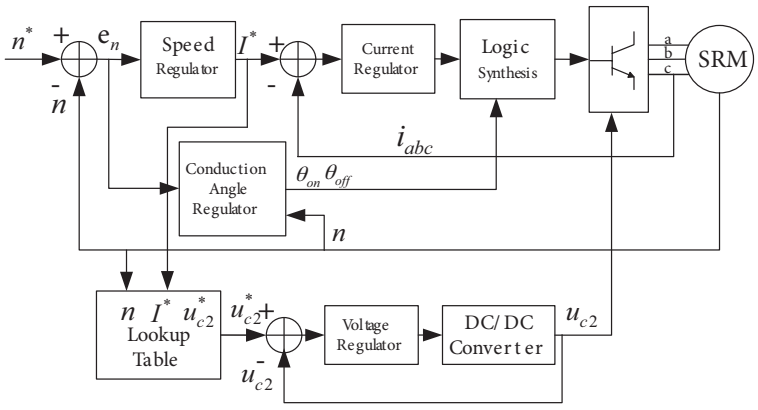

Figure 8. Control structure diagram for the driving state.

When a SRM works at low speed with a low load, a lower DC-link voltage can be used to reduce switching frequency, switching losses, and switching noise, and to optimize chopping current waveforms. At high speed, a higher DC-link voltage can be used to reduce magnetization and demagnetization time, and to decrease the effect of the back EMF as well as increase the power output. Speed n, reference I^*, and reference DC-link voltage u_{c2}^* are stored in a lookup table. The front-end DC/DC converter is regulated by a voltage regulator to make the DC-link voltage follow the reference voltage u_{c2}^*. When the speed is greater than 2800 rpm, u_{c2}^* is set at 120 V; when the speed is less than 2800 rpm, u_{c2}^* is increased as speed n and reference I^*. The lookup table is created by the experiment and is shown in Table 1.

Table 1. n(rpm), I^* (A), u_{c2}^* (V) lookup table.

n \ I^*	10	20	30	40	50	60	70	80	90	100
100	48	48	49	50	50	51	51	52	52	53
200	49	49	49	50	50	51	52	52	53	53
300	49	50	50	51	51	52	52	53	54	54
400	49	50	50	51	51	52	53	53	54	54
500	50	50	51	52	52	53	53	54	55	55
600	52	52	53	55	57	57	58	58	58	59
700	55	55	58	59	60	60	61	61	62	63
800	57	62	76	77	79	80	80	81	81	82
900	58	69	76	78	79	81	81	82	82	83
1000	64	75	78	80	80	82	83	83	84	84
1200	84	92	93	93	94	94	94	95	95	95
1400	98	98	98	99	99	100	100	100	101	101
1600	101	101	101	102	102	102	103	103	104	104
1800	104	104	104	105	105	105	106	106	106	107
2000	106	106	107	107	107	108	108	109	109	109
2200	108	108	108	109	109	109	110	110	110	111
2400	111	111	111	112	112	113	113	113	113	114
2600	114	114	114	115	115	115	116	116	116	117
2800	118	118	118	118	119	119	119	120	120	120
>2800	120	120	120	120	120	120	120	120	120	120

4.2. Control strategy for the braking state

When an EV is in the braking state, a SRM, serving as a generator, converts the kinetic energy into electrical energy. CCC is adopted at low speed; the turn-on angle is at θ_a, and the turn-off angle is at θ_m. At high speed, APC is applied, θ_{on} is fixed at θ_a, and the braking torque is regulated by changing the value of θ_{off} [15].

A SRM is a single-sided excitation machine; it needs initial excitation energy to implement regenerative braking. In order to ensure the stability of the excitation voltage and flexible control of the transfer between excitation energy flow and braking energy flow, DC-link voltage u_{c2} is chosen to be the control variable.

When u_{c2} is greater than the given value of 98 V, the regenerative braking energy is larger than the excitation energy; in this case, regulator α is chosen. Hence, the battery is charged by controlling switch T_2. The system is in a regenerative braking state until the DC-link voltage is smaller than the given value. When u_{c2} is smaller than the given value 94 V, the excitation energy is larger than the regenerative braking energy; in this case, regulator 1 is chosen. Excitation energy should be increased by controlling switch T_1 to maintain the DC-link voltage constant. The 2 modes automatically switch by detecting DC-link voltage u_{c2}. Meanwhile, hysteresis is added to reduce switching chattering. The control structure diagram is shown in Figure 9.

4.3. Control strategy for charging state

When EV works in the charging state, a PFC circuit converts AC into DC with a high power factor, and then the battery is charged by a buck circuit. The battery is charged by 2-stage charging. That is, the first stage is constant current charging and the second stage is constant voltage charging. In this way, an optimal charging characteristic can be obtained.

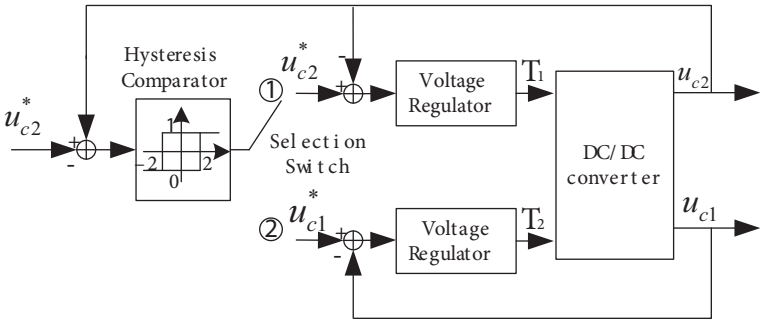

Figure 9. Control structure diagram for the braking state.

As shown in Figure 10a, the external voltage loop and internal current loop are applied to a PFC circuit. The voltage regulator makes C_2 voltage follow the reference voltage u_{c2}^* and then outputs the amplitude of the reference current I_{ac}^*. Unit AC voltage is multiplied by I_{ac}^* to get the reference current $I_{ac}^* sin\omega t$. An internal current regulator makes the actual current follow the reference current $I_{ac}^* sin\omega t$.

As shown in Figure 10b, the 2-stage charging method is achieved by a buck converter. When the battery voltage is smaller than 45 V, constant current charging begins. The charging current is 20 A. When the battery voltage is larger than 45 V, constant voltage charging begins.

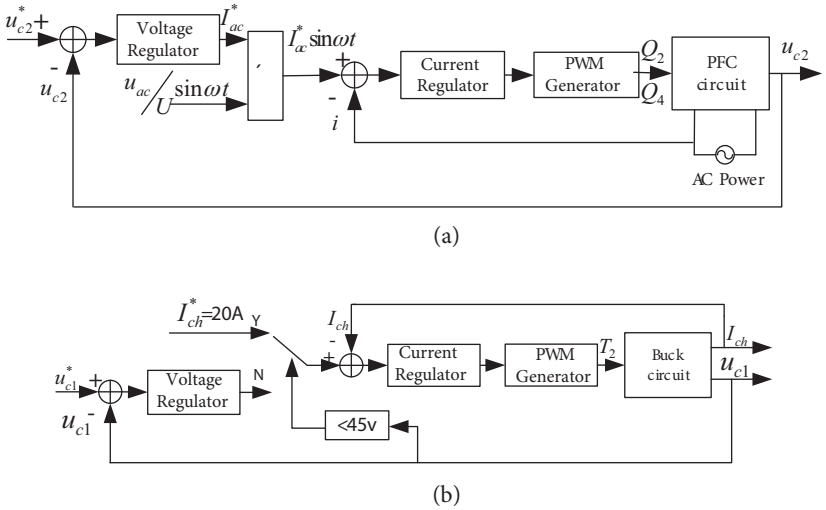

Figure 10. Control structure diagram for the charging state: (a) PFC, (b) charging battery.

5. Selection of the drive topology components

The parameters of the SRM are shown in Table 2.

5.1. Selection of storage inductor and filter capacitor of a bidirectional DC/DC converter

When a SRM works at a rated point, the battery voltage is 48 V. The rated converter output current I_o is 78.12 A, according to the parameters in Table 2. When the front-end DC/DC converter is operated under the continuous-condition mode [16],

$$I_{Ld} = \frac{I_o}{1 - D}, \tag{1}$$

Table 2. Specifications of the SRM.

Parameter	Value
Phases	3
Stator poles	12
Rotor poles	8
Rated power (kW)	7.5
Rated voltage (V)	96
Rated speed (rpm)	1200
Max. inductance (mH)	7.32
Min. inductance (mH)	1.07

$$L_d = \frac{u_{c1}(u_{c2} - u_{c1})}{u_{c2}\Delta i_L f_s}, \tag{2}$$

where I_{Ld} is the inductor current, D is the duty cycle, f_s is the switching frequency, and Δi_L is the inductor ripple current.

When f_s is set to 12 kHz, the maximum ripple amplitude value is 5% of the nominal current, and the L_d inductance value has to be set to at least 512 μH.

$$C_1 \geq \frac{\Delta i_L}{8 f_s \Delta u_{c1}} \tag{3}$$

$$C_2 \geq \frac{I_{o(\max)}(u_{c2} - u_{c1})}{\Delta u_{c2} f_s u_{c2}} \tag{4}$$

$I_{o(\max)}$ is the maximum of the load current, Δu_{c1} is the ripple voltage of C_1, and Δu_{c2} is the ripple voltage of C_2.

Δu_{c1} is set at 0.5 V; Δu_{c2} is set at 1.5 V. Assuming $I_{o(\max)}$ is the double of I_o, then C_1 must be greater than 81.4 μF and C_2 must be greater than 4340 μF. Therefore, an electrolytic capacitor with a rated value of 100 μF and a rated voltage of 400 V is chosen for C_1; an electrolytic capacitor with a rated value of 4700 μF and a rated voltage of 400 V is chosen for C_2.

5.2. Selection of power switches

Insulated gate bipolar transistors (IGBT) GA300RD60U and GA300LD60U made by the IR Company are chosen for power switches, which can withstand voltage of 600 V and current of 300 A.

5.3. Parameters of the charging circuit

The power source is V_{ac} = 110 V / 50 Hz, and the amplitude of V_{ac} is V_m = 156 V. If the maximum voltage across the winding is 156 V while ignoring winding resistance and the conduction voltage drop of switches, then:

$$\Delta i = \frac{u}{L f_c}. \tag{5}$$

Here f_c is the chopping frequency when in the charging state, which is set at 30 kHz. When Δi is 5 A, L = 1.04 mH $< L_{\min}$ = 1.07 mH. Therefore, the inductance value of the SRM winding satisfies the needs of the charging circuit. The maximum value of the charging current is 20 A, and IGBT capacity also meets the needs of the charging circuit.

6. Experimental platform and experiments

In order to verify the proposed drive topology and control strategies, an experimental platform is built as shown in Figure 11. Figure 11 shows the converter, control board, driver board, and dual-motor system. The dual-motor system simulates the driving state and braking state of the EV. When in the charging state, the SRM is locked.

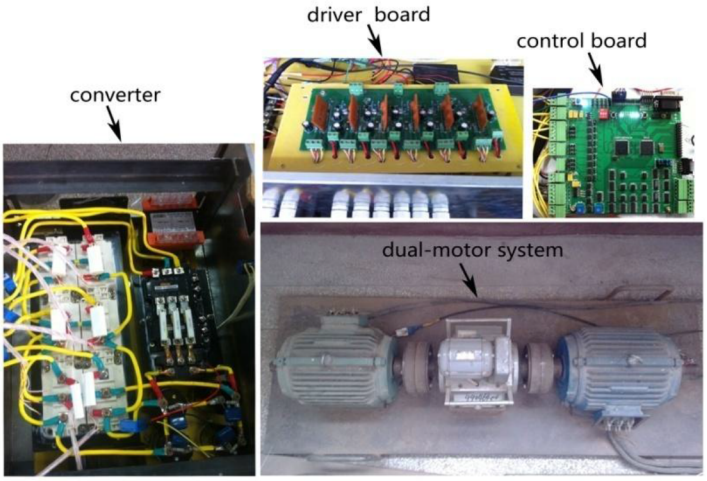

Figure 11. Photograph of the experimental platform.

6.1. Driving state experiments

Figures 12–14 show the experimental waveforms of the driving state of the EV.

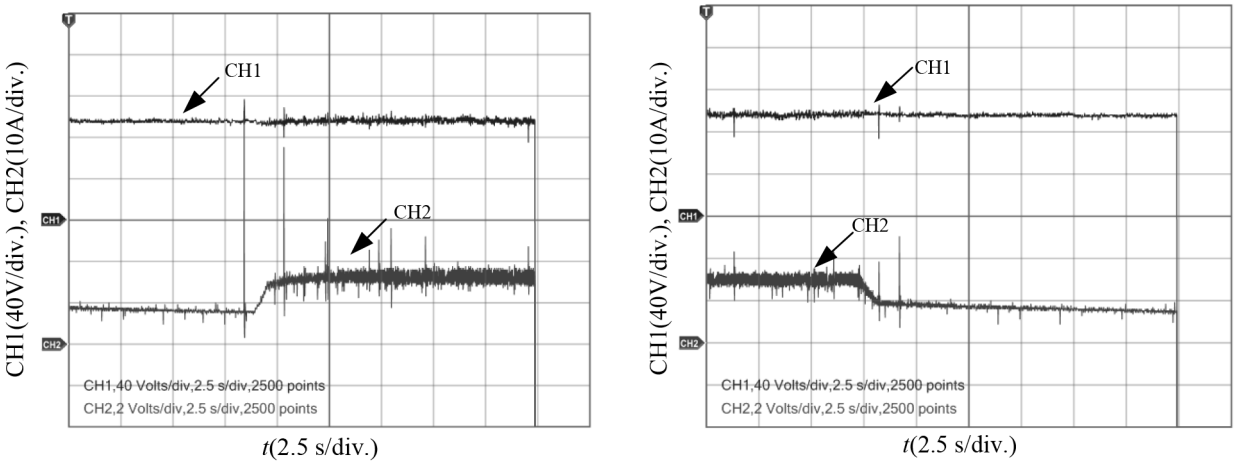

Figure 12. C_2 voltage and battery output current waveforms: (a) increasing the load, (b) decreasing the load.

As shown in Figure 12, channel CH1 is the voltage waveform of capacitor C_2 and channel CH2 is the output current waveform of the battery. The voltage ripple of capacitor C_2 is small when SRM increases the load in Figure 12a or decreases the load in Figure 12b, which can reduce the influence of battery voltage fluctuation on the performance of the SRM.

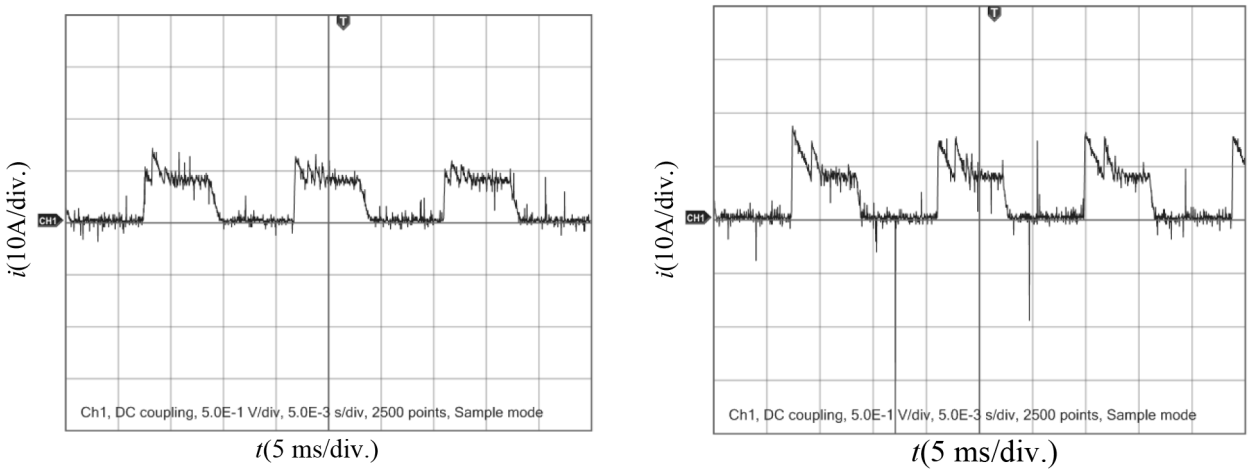

Figure 13. The 600 rpm phase current waveforms during the driving state: (a) 52 V, (b) 96 V.

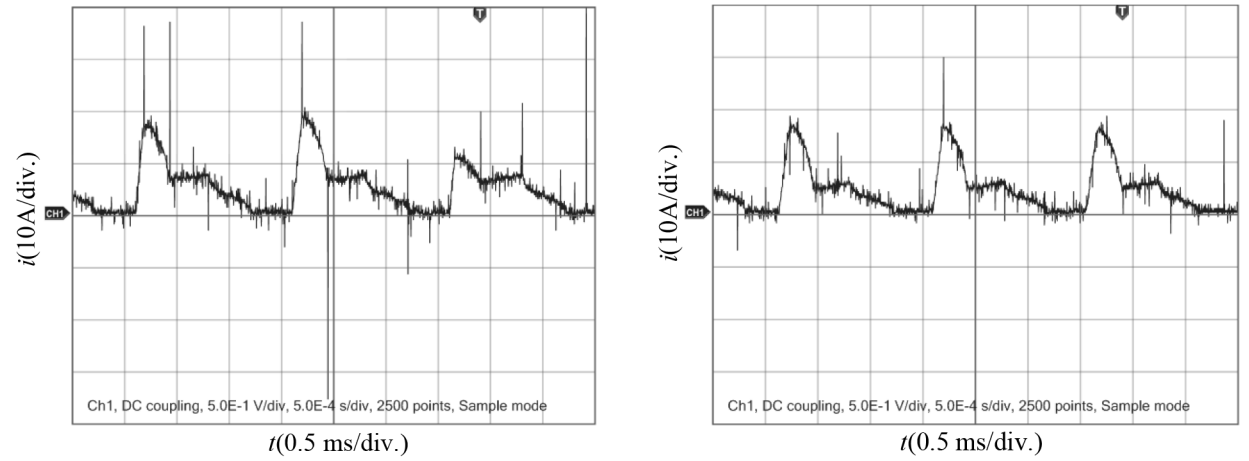

Figure 14. The 5600 rpm phase current waveforms during the driving state: (a) 120 V, (b) 96 V.

At low speed with a low load, the phase current can be optimized, chopping frequency will be cut down, and switching losses are reduced by reducing the DC-link voltage. The phase current waveform is smoother when the DC-link voltage is set at 52 V in Figure 13a as compared to when the DC-link voltage is set at 96 V in Figure 13b.

At high speed, DC-link voltage is not sufficient to force the actual current to follow the reference current since the back EMF is large, so the output power decreases. The power output capability can be improved through boosting the battery voltage. The increase of the phase current in the DC-link voltage of 120 V in Figure 14a is higher than that of a DC-link voltage of 96 V in Figure 14b.

6.2. Braking state experiments

Figure 15 shows the experimental waveforms when a SRM works in the braking state. Figures 16 and 17 show the experimental waveforms when the SRM switches from driving state to braking state.

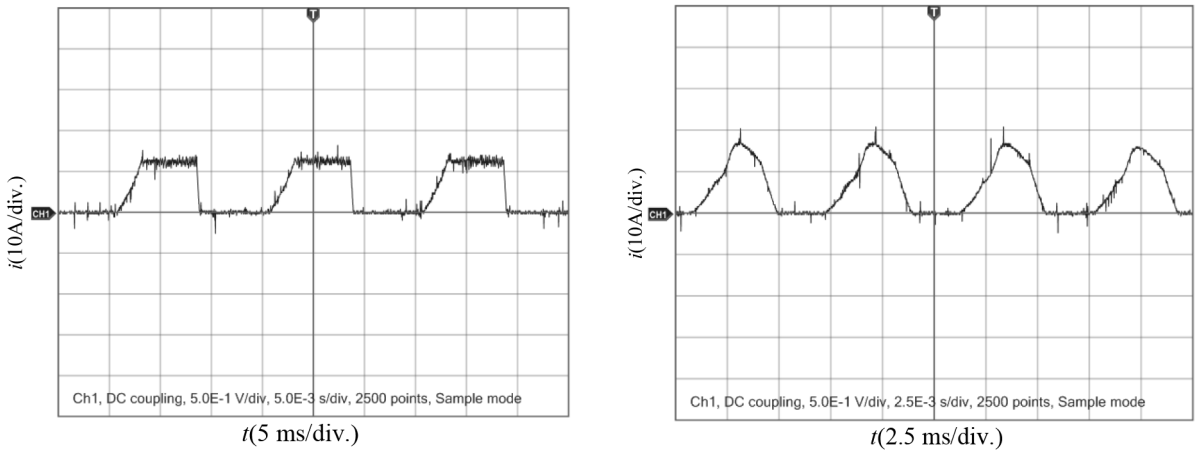

Figure 15. Phase current waveforms during the braking state: (a) 500 rpm, (b) 1500 rpm.

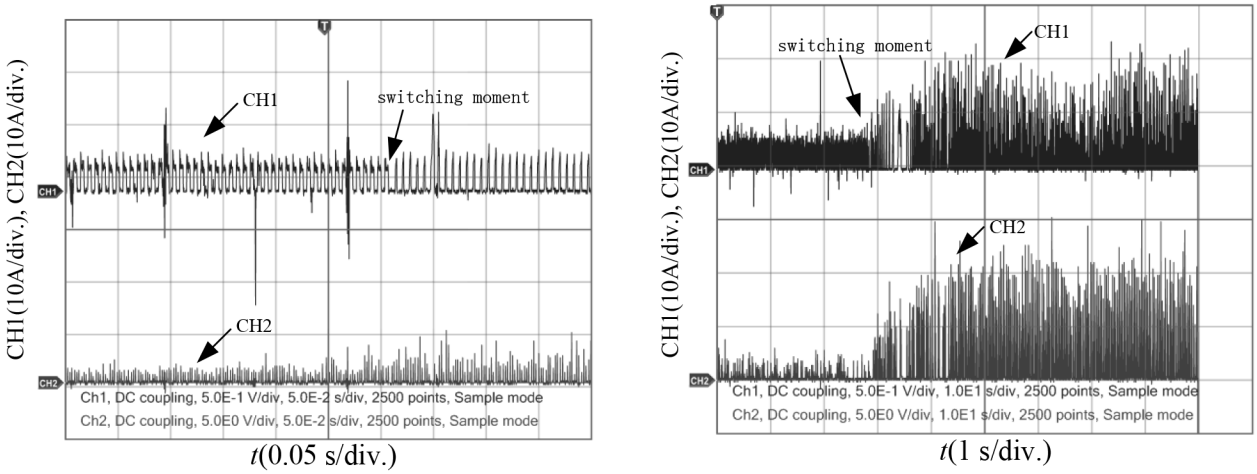

Figure 16. Phase current and freewheeling diode current waveforms occurring from the driving state to the braking state: (a) horizontal axis 0.05 s/div, (b) horizontal axis 1 s/div.

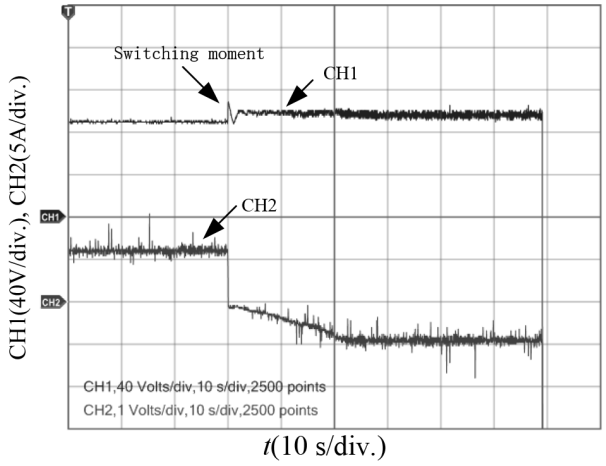

Figure 17. C_2 voltage and battery current waveform occurring from the electric state to the braking state.

As shown in Figure 15a, when the SRM works at low speed, CCC is adopted. The braking current waveforms are symmetrical with the driving current waveforms. The reference I^* is regulated to change the braking torque. At high speed, APC is adopted, and only the turn-off angle θ_{off} is regulated to change the braking torque. The braking current waveforms for high speed are shown in Figure 15b.

As shown in Figure 16, channel CH1 is the phase current waveform of the SRM, and channel CH2 is the current (feedback current) waveform of the freewheeling diode. When the braking signal is given, the turn-on and turn-off angles are changed. The phase current turns into a braking current, as shown in channel CH1. As shown in channel CH2, the feedback current increases as the braking signal increases. Thus, the conversion energy increases between the electrical energy and the kinetic energy.

As shown in Figure 17, channel CH1 displays the voltage waveform of capacitor C_2, and channel CH2 shows the current waveform of the battery. In the driving state, the battery discharges. When the braking signal is given, the voltage of capacitor C_2 increases. The electric state switches into braking state automatically by detecting the voltage of C_2. In the meantime, the 2 voltage regulators keep the voltage of the 2 capacitors stable. The battery-charging current increases as the braking signal increases and finally reaches the given charging current.

6.3. Charging state experiments

Figures 18 and 19 show the experimental waveforms of the charging state of the EV. When switches Q_1, Q_2, Q_3, and Q_4 are turned off, diodes D_1, D_2, D_3, and D_4 constitute a noncontrolled rectifier bridge. Voltage and current waveforms of AC power are shown in Figure 18a. The current and voltage are not in phase. Current waveforms are similar to the triangle wave. When the proposed PFC circuit is adopted, voltage and current waveforms are as shown in Figure 18b. The current is in phase with the voltage, and the current waveforms are similar to a sine wave, so the power factor is high. Figure 19 shows the phase current FFT analysis of the 2 methods.

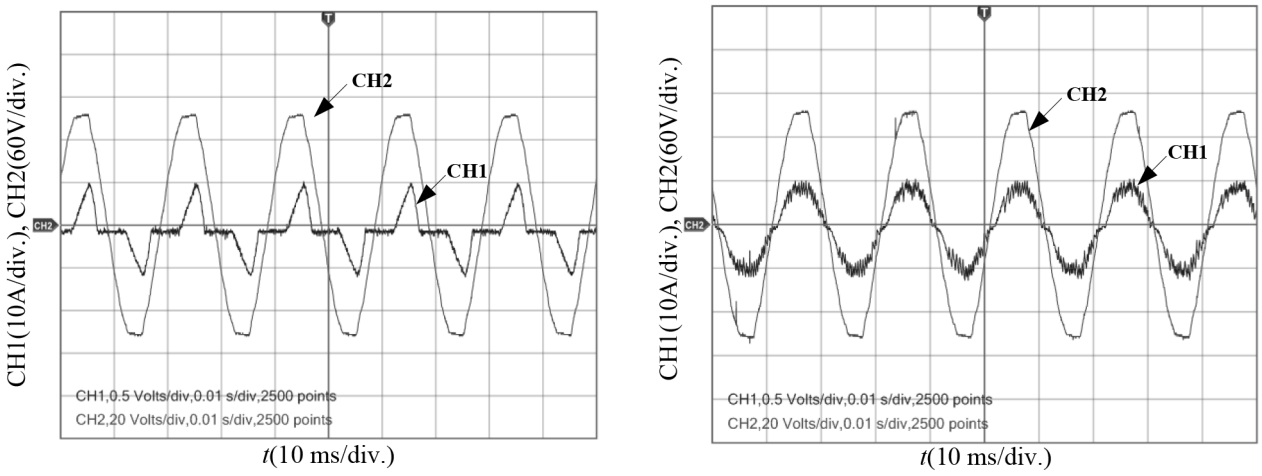

Figure 18. Grid voltage and current waveforms: (a) diode rectifier waveforms, (b) PFC circuit rectifier waveforms.

As shown in Figure 19a, the current contains 3rd, 5th, 7th, and 9th harmonics. The power factor is 0.873 and the total harmonic distortion (THD) is 43.9%. As shown in Figure 19b, when the PFC circuit is utilized, the harmonic contents are reduced and the power factor is improved. The power factor is 0.982 and the THD is 7.82%. Therefore, the proposed PFC circuit reduces the impact of the load on the grid.

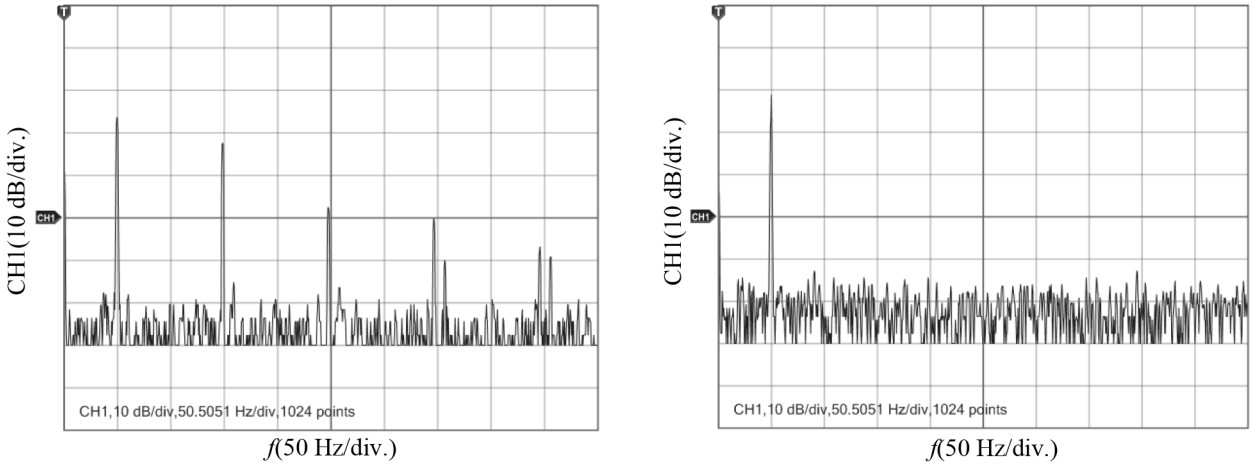

Figure 19. FFT analysis of current waveforms: (a) diode rectifier, (b) PFC rectifier.

7. Conclusion

A drive topology that can achieve 3 working states is proposed. In the driving state, the DC-link voltage is real-time adjusted to implement low loss and low noise at low speed and enhance the power output capability at high speed, based on the operating characteristics of the SRM. In the braking state, excitation and braking energy feedback automatically switch by detecting the DC-link voltage to implement a bidirectional flow of energy. In the charging state, SRM windings and a power converter are employed to constitute an onboard charger with the function of a PFC. A 2-stage charging method is applied to charge the battery. Control strategies are put forward and verified by experiments according to the 3 working states.

Acknowledgment

This work was supported in part by the National Natural Science Foundation of China under Grant No. 51277174.

References

[1] Ehsani M, Gao Y, Emadi A. Modern Electric, Hybrid Electric and Fuel Cell Vehicles: Fundamentals, Theory, and Design. 2nd ed. New York, NY, USA: CRC Press, 2010.

[2] Hartani K, Bourahla M, Miloud Y, Sekour M. Electronic differential with direct torque fuzzy control for vehicle propulsion system. Turk J Electr Eng Co 2009; 17: 21–38.

[3] Krishnan R. Switched Reluctance Motor Drives: Modeling, Simulation, Analysis, Design, and Applications. Boca Raton, FL, USA: CRC Press, 2001.

[4] Yahia H, Liouane N, Dhifaoui R. Multiobjective differential evolution-based performance optimization for switched reluctance motor drives. Turk J Electr Eng Co 2013; 21: 1061–1076.

[5] Inderka RB, Menne M, Doncker RWAAD. Control of switched reluctance drives for electric vehicle applications. IEEE T Ind Electron 2002; 49: 48–53.

[6] Xue XD, Cheng KWE, Lin JK, Zhang Z, Luk KF, Ng TW, Cheung NC. Optimal control method of motoring operation for SRM drives in electric vehicles. IEEE T Veh Technol 2010; 59: 1191–1204.

[7] Takeno M, Chiba A, Hoshi N, Ogasawara S, Takemoto M, Rahman MA. Test results and torque improvement of the 50-kW switched reluctance motor designed for hybrid electric vehicles. IEEE T Ind Appl 2012; 48: 1327–1334.

[8] Rahman KM, Fahimi B, Suresh G, Rajarathnam AV, Ehsani M. Advantages of switched reluctance motor applications to EV and HEV: design and control issues. IEEE T Ind Appl 2000; 36: 111–121.

[9] Chen H, Gu JJ. Implementation of the three-phase switched reluctance machine system for motors and generators. IEEE/ASME T Mech 2010; 15: 421–432.

[10] Ronanki D, Parthiban P. PV-battery powered direct torque controlled switched reluctance motor drive. In: IEEE 2012 Power and Energy Engineering Conference; 27–29 March 2012; Shanghai, China. New York, NY, USA: IEEE. pp. 1–4.

[11] Ortuzar M, Moreno J, Dixon J. Ultracapacitor-based auxiliary energy system for an electric vehicle: implementation and evaluation. IEEE T Ind Electron 2007; 54: 2147–2156.

[12] Solero L. Nonconventional on-board charger for electric vehicle propulsion batteries. IEEE T Veh Technol 2001; 50: 144–149.

[13] Weng KT, Pollock C. Low-cost battery-powered switched reluctance drives with integral battery-charging capability. IEEE T Ind Appl 2000; 36: 1676–1681.

[14] Sul SK, Lee SJ. An integral battery charger for four-wheel drive electric vehicle. IEEE T Ind Appl 1995; 31: 1096–1099.

[15] Narla S, Sozer Y, Husain I. Switched reluctance generator controls for optimal power generation and battery charging. IEEE T Ind Appl 2012; 48: 1452–1459.

[16] Erickson RW. Fundamentals of Power Electronics. New York, NY, U SA: Chapman and Hall, 1997.